SAND2007-8138C

Accurate Measurement of Cellular Autofluorescence is Critical for Imaging of Host-Pathogen Interactions

Jerilyn A. Timlin[a*], Rachel M. Noek[a], Julia N. Kaiser[b], Michael B. Sinclair[a], Howland D. T. Jones[a], Ryan W. Davis[a], Todd W. Lane[b]
[a]Sandia National Laboratories, 1515 Eubank Blvd SE, Albuquerque, NM, USA 87123;
[b]Sandia National Laboratories, 7011 East Avenue, Livermore, CA USA 94550

ABSTRACT

Cellular autofluorescence, though ubiquitous when imaging cells and tissues, is often assumed to be small in comparison to the signal of interest. Uniform estimates of autofluorescence intensity obtained from separate control specimens are commonly employed to correct for autofluorescence. While these may be sufficient for high signal-to-background applications, improvements in detector and probe technologies and introduction of spectral imaging microscopes have increased the sensitivity of fluorescence imaging methods, exposing the possibility of effectively probing the low signal-to-background regime. With spectral imaging, reliable monitoring of signals near or even below the noise levels of the microscope is possible if autofluorescence and background signals can be accurately compensated for. We demonstrate the importance of accurate autofluorescence determination and utility of spectral imaging and multivariate analysis methods using a case study focusing on fluorescence confocal spectral imaging of host-pathogen interactions. In this application fluorescent proteins are produced when bacteria invade host cells. Unfortunately the analyte signal is spectrally overlapped and typically weaker than the cellular autofluorescence. In addition to discussing the advantages of spectral imaging for following pathogen invasion, we present the spectral properties of mouse macrophage autofluorescence. The imaging and analysis methods developed are widely applicable to cell and tissue imaging.

Keywords: Hyperspectral imaging, spectral imaging, fluorescence imaging, confocal, autofluorescence, spectral crosstalk, multivariate analysis, multivariate curve resolution, MCR, fluorescent proteins.

1. INTRODUCTION

Fluorescence microscopy is a powerful tool for imaging proteins and their interactions in cells. As bioscience researchers look deeper into the details of cellular machinery there is an increasing need to monitor lower and lower levels of protein expression. The fundamental limit on sensitivity in the fluorescence microscope is often not the signal to noise ratio, but rather the signal to background ratio. This background signal arises from spectrally interfering species such as additional labels used in a multicolor experiment, cell growth media, and/or cellular autofluorescence that emit photons in the same spectral range as the analyte of interest, thus contaminating the signal. This phenomenon is commonly referred to as spectral crosstalk or spectral bleed through (SBT). For intense analyte signals, low levels of background interference can be tolerated, but as the analyte signal approaches the detection limit of the microscope as it often does in realistic experiments, accurate measurement and compensation for contaminants are required. Correction for the contaminating fluorescence in fluorescence microscopy has been demonstrated through the use of independent control images and can require up to seven independent images for fluorescence resonance energy transfer (FRET) based measurements.[1] In practice the use of control images is tedious and often the fluorescent properties of the interferrant are highly variable and may change with different experimental conditions leading to insufficient background correction. Correcting for cellular autofluorescence can be particularly problematic because of its non-uniform intensity distribution within and between cells, as well as across cell lines. The development of spectral imaging technology and accompanying spectral unmixing algorithms have promise to alleviate this limitation.[2-7] Spectral imaging systems use the entire spectral signature of a fluorescent species to generate images rather than the univariate intensity used in traditional fluorescence microscopy. This provides a sensitivity and specificity advantage if the spectra of all the fluorescing species in an image are accurately modeled using multivariate image analysis. If background fluorescence signal is left unmodeled it can reduce the performance of spectral unmixing algorithms. Spectral imaging has been

* jatimli@sandia.gov, Phone: (505) 844-7932, fax: (505) 284-3775

shown to be effective in removing the effects of autofluorescence for biomedical applications.[8, 9] We have previously demonstrated the utility of spectral imaging for removing contaminating fluorescence in DNA microarrays[10, 11] and addressed the importance of modeling all the fluorescent species in multicolor imaging of brain tissue.[12]

In our current application we are interested in visualizing low levels of protein expression and protein-protein interactions to improve our understanding of virulence mechanisms in the potential biowarfare agent *Francisella tularensis*. For these studies we are using *F. tularensis* subspecies *novicida* strain U112 (hereafter *F. novicida*) which displays reduced virulence in humans but full virulence in mice. The virulence mechanism of *F. tularensis* has been recently shown to include a novel Type VI secretion system (T6SS) which appears to be conserved in all subspecies.[13] Our efforts aim to develop advanced molecular biology strategies and low-light imaging methodologies to permit us to assess spatial and temporal patterns of *F. novicida* virulence proteins during host cell infection. We have chosen for our initial targets the virulence proteins IglA and IglB. These proteins are conserved in all subspecies of F. tularensis and are thought to play a structural role in the formation of the T6SS. In order for us to provide simultaneous quantification of multiple fluorescent proteins, we have employed a custom built confocal spectral microscope [14] and optimized our multivariate curve resolution (MCR) algorithms to separate the highly overlapped spectra. The resulting fluorescence intensities of the biological processes we are interested in have weak signals, unfortunately often weaker than the native host cell autofluorescence emission, thus it is critical that we fully understand the impact of autofluorescence on our measurements. Our approach provides a tool not only for investigating autofluorescence but also for eliminating its effect on imaging of virulence protein interactions.

2. METHODOLOGY

2.1 Strains and growth conditions.

Francisella tularensis subspecies *novicida* strain Utah 112 (BEI Resources NR-13) was used to generate all transformants in this study. Unless otherwise specified, bacteria were grown in tryptic soy broth (BBL 211768) or tryptic soy agar (BBL 211043) supplemented with 0.1% cysteine (TSBC and TSAC). When required, kanamycin (10 μg/mL) was used. Single bacterial colony isolates were grown in TSBC to mid-log phase. Sterile glycerol was added to 20%, and 0.5mL aliquots were frozen and stored at -80ºC. Freshly-thawed aliquots were used for all infection experiments and were titered by plating dilutions on TSAC plates and counting colonies.

The murine macrophage-like cell line RAW264.7 (ATCC TIB-71) were used as the host for F. novicida infections int these studies. RAW264.7 cells were grown in non-treated culture flasks (Nunc 156800) in "RAWGM1," DMEM (ATCC 30-2002) supplemented with 10% heat-inactivated FBS (Gemini Bio-Products 100-500), 20mM HEPES (Invitrogen 15630080), and 2mM L-Glutamine (Invitrogen 25030081) at 37ºC, 5% CO2.

2.2 Fluorescent proteins.

The *Francisella* shuttle plasmid pFNLTP6 and pFNLTP6-groE-GFP were gifts from Thomas Zahrt of the Medical College of Wisconsin. A cassette containing the *F. novicida* U112 iglA and iglB genes was synthesized *de novo* by Epoch Biolabs, Inc., and was cloned into the KpnI/BamHI sites of pFNLTP6. For this study, the mTangerine and mHoneydew genes were synthesized *de novo* following codon optimization for expression in *Francisella*. In-frame fusions of mHoneydew at the amino terminus of iglA and mTangerine at the amino terminus of igl B were generated using standard cloning techniques.

2.3 Bacterial transformation.

Plasmid DNA was introduced into *F. novicida* U112 by chemical transformation as previously described.[15] Bacteria were first streaked onto day-old TSAC plates supplemented with 0.4% glucose and then transferred to TSBC media with 0.4% glucose and were grown to mid- to late- log phase. Cells were pelleted at 4300 RPM for 15 minutes and resuspended in 2mL transformation buffer. Ten microliters of plasmid was mixed with 500μL cell suspension and incubated at 37ºC for 20 minutes without shaking. After addition of 1mL TSBC/glucose, tubes were shaken for 2 hours at 37ºC at 200 RPM. 50-200uL of mix was plated on fresh TSAC/glucose selection plates. Colonies appeared after several days incubation at 37ºC.

2.4 Infection of RAW264.7 cells with bacteria.

RAW264.7 cells were infected with *F. novicida* U112 transformants as follows: 10^5 RAW264.7 cells were seeded per well into 4 well chamberslides or chambered coverglasses (NNI 154917, 155382) in RAWGM1 one day prior to

infection. Bacteria were opsonized in 10% mouse complement serum (Innovative Research IMS-COMPL) for 30 minutes at 37ºC for one hour immediately prior to use. Cells were infected with *F. novicida* U112 transformants at an input ratio of 10-50 bacteria per cell in 0.5mL RAWGM1 per well. Chamberslides were centrifuged at 300g for 5 minutes at 4ºC to promote bacterial adherence to the cells. Following an ingestion incubation of 1 hour at 37ºC, 5% CO2, adherent cells were gently washed 3times with RAWGM; a final 1 mL of RAWGM1 was added per well. Samples were fixed at various times post infection in 4% paraformaldehyde for 30 minutes, followed by 3 PBS washes. Chamberslides were prepared for microscopy by mounting #1.5 glass coverslips in ProLong Gold Antifade reagent (Invitrogen P36934) and sealed.

2.5 Spectral image acquisition

Spectral image data were collected using a scanning confocal hyperspectral microscope described by Sinclair et al[14]. In this system, fluorescence emission is excited by a continuous wave 488nm laser and collected from 500nm to 800nm using a prism-based EMCCD spectrometer at each point. Vertical binning of the spectral data in 512 EMCCD pixels combined with a push broom readout mode[16] allows data collection to be performed at a maximum sustained readout rate of 8.3 Mbits/s at a spectral resolution >3nm. In the described experiments, low resolution imaging was performed using an infinity corrected 20x objective (Nikon, PlanApo NA = 0.75), corresponding to an in-plane voxel dimension of 0.24μm per side. High resolution imaging was performed using an infinity corrected 60x oil-immersion objective (Nikon, PlanApo VC NA = 1.40), corresponding to an in-plane voxel dimension of 0.12μm per side. In both cases, 204 x 204 point spectral arrays were collected at a scan rate of 4167 spectra per second, for an overall single image collection time of ~10 sec.

2.6 Data pretreatment and analysis

All data were preprocessed and analyzed using dual-processor desktop computers and custom written code in Matlab (Mathworks, Inc.) or C++. The preprocessing of the spectral image data consisted of four steps. First, the image data was interrogated for cosmic spikes that may have been inadvertently collected on the detector. If the software finds a spectrum that contains a cosmic spike, the entire spectrum (voxel) is replaced with a spectrum from an adjacent voxel. Next, a dark image is subtracted from the image data. The dark image is collected near in time to the image data and is of the same spatial size as the image data. The dark image is typically a rank one dataset (i.e., the majority of this dataset can be explained using one eigenvector when a Principle Component Analysis (PCA) is conducted). Since the dark image data is rank one, the contributions of the first eigenvector from the image data are simply subtracted from the image data and thereby prevent any inflation in noise on the image data. Next, the offset that arises from the electronics of the EMCCD detector is removed from the image data on a per voxel basis. Since the first twenty spectral channels in the spectrum are absent of light (due to a cutoff filter), averaging across these channels can provide a good estimate of the amount of offset to subtract. Finally, these data were weighted for both Poisson and read noise emanating from the EMCCD. Details describing Poisson noise weighting for time-of-flight secondary ion mass spectrometry images is described elsewhere.[17] In addition a manuscript describing the Poisson and read noise weighting for fluorescence images is in preparation.

Following the preprocessing of the image data, the analysis of the image data consisted of using MCR to obtain the pure spectral components and corresponding intensities of the image data. MCR is a powerful analysis technique that requires little or no knowledge of the dataset and when combined with hyperspectral imaging can separate and quantify many overlapping fluorophores. Details of the MCR analysis are published elsewhere.[18-20] MCR is initialized with the number of pure spectral components to calculate during the analysis and with the initial estimates of the pure spectral components. PCA was used to determine the number of non-noise related spectral components present in our image data. When dealing with unknown datasets, our spectral pure component estimates are typically random numbers to initialize MCR, however when spectral components are known or suspected, it is best to start with those estimates instead. For these image data a preliminary MCR analysis was initiated with random numbers and composite images consisting of individual images of the same type. (i.e. one “super-image” containing all the images of unlabeled living cells, another contained all images of macrophages 7.5 hr post-infection with IglB::mTangerine *F. novicida*, etc.). In the MCR analysis the spectral estimates were normalized to unit length to ensure algorithm stability. The results were unweighted and PCA of the weighted spectral residuals was performed to confirm the adequacy of fit of the model to the image data. Once good spectral estimates are obtained from MCR, a CLS analysis was performed using the results of the MCR analysis rescaled to maximum emission = 1. This was done to facilitate interpretation and ease direct visual comparison of relative intensities.

3. RESULTS

Figure 1 contains the pure component spectral estimates from MCR analyses of hyperspectral images containing *F. novicida* expressing fluorescent proteins (mTangerine, mHoneydew, GFP) and typical macrophage autofluorescence. These spectra were obtained from multiple images from separate experiments of *F. novicida* challenged cells and are normalized to maximum intensity and overlaid for comparison. It is clear that the macrophage autofluorescence is spectrally overlapped with these fluorescent proteins and would confound attempts to visualize protein localization patterns without the extra dimension of spectral information. It should also be noted that, although not the subject of this proceedings, the fluorescent proteins themselves are spectrally congested and contribute spectral crosstalk with each other, requiring spectral imaging to use these in a multicolor experiment.

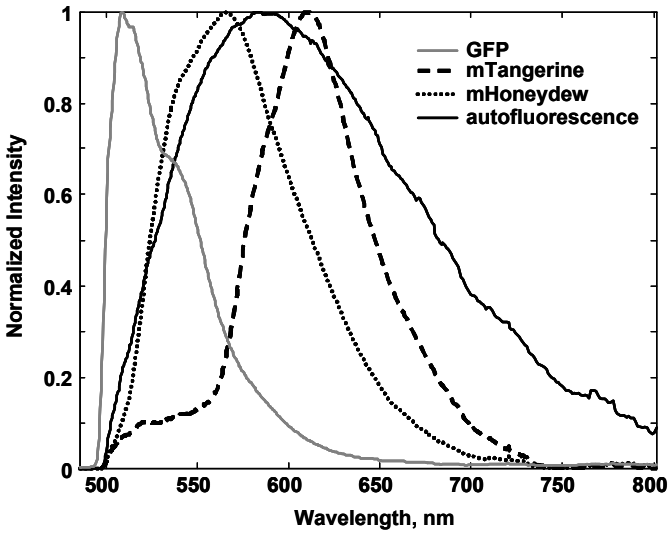

Fig. 1. MCR extracted spectral signatures of fluorescent protein fusions (solid gray trace = groE::GFP, dotted black trace = mHoneydew::IglA, dashed black trace = mTangerine::IglB) and macrophage autofluorescence (solid black trace) demonstrating high degree of spectral overlap. Spectra have been normalized to a maximum peak =1.

Typical concentration maps corresponding to macrophage autofluorescence and *groE*::GFP expression following an overnight infection of RAW cells with *F. novicida* containing the *groE*::GFP construct are shown in Figure 2b and 2c, respectively. For comparison, the total intensity image is shown in Figure 2a and corresponds more closely to what might result from a filter-based microscope equipped with a GFP filter. Focusing on the two areas indicated by the arrowheads illustrates a common problem. Without information from the spectra of the fluorescent species one is forced to look for patterns in this total intensity image that resemble expectations of infecting bacteria. The areas indicated by the arrows appear very similar and would likely be incorrectly assigned to invading bacteria. Conversely, the MCR analysis of this image successfully separates these images into its two underlying fluorescent components and independent concentration maps are calculated for each species (GFP, Fig. 2c; macrophage autofluorescence, Fig. 2b). These maps provide a clearer understanding of the spatial distribution of the fluorescent protein versus macrophage autofluorescence. While one of the arrowheads does point to an area of *groE*::GFP expression, the other points to an area of more concentrated macrophage autofluorescence.

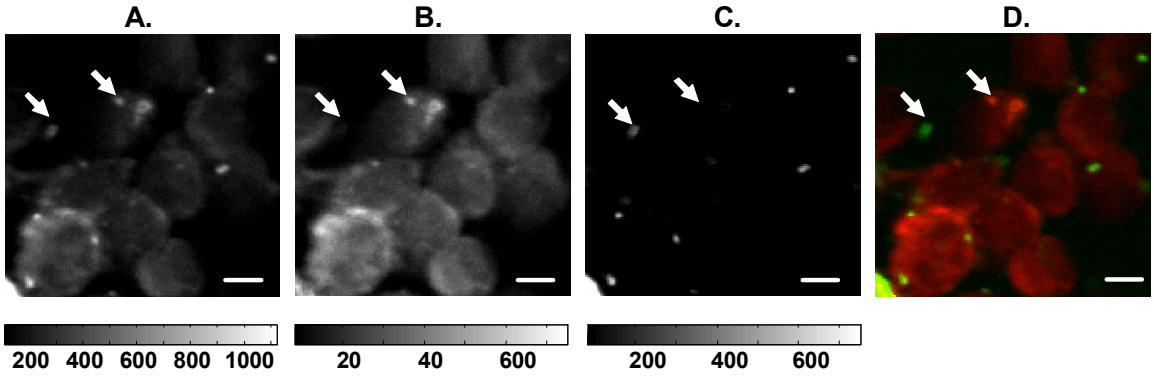

Fig. 3. Spatial distribution of *groE*::GFP expression in *F. novicida* infected cells. Cells were fixed following infection and prior to imaging. A. Total summed intensity image. B. MCR extracted concentration map of macrophage autofluorescence C. MCR extracted concentration map of *groE*::GFP expression. Arrowheads indicate areas of interest and are in the same position in each panel. D. Color overlay of B. & C. Color available on-line only. Scale bar = 5 μm.

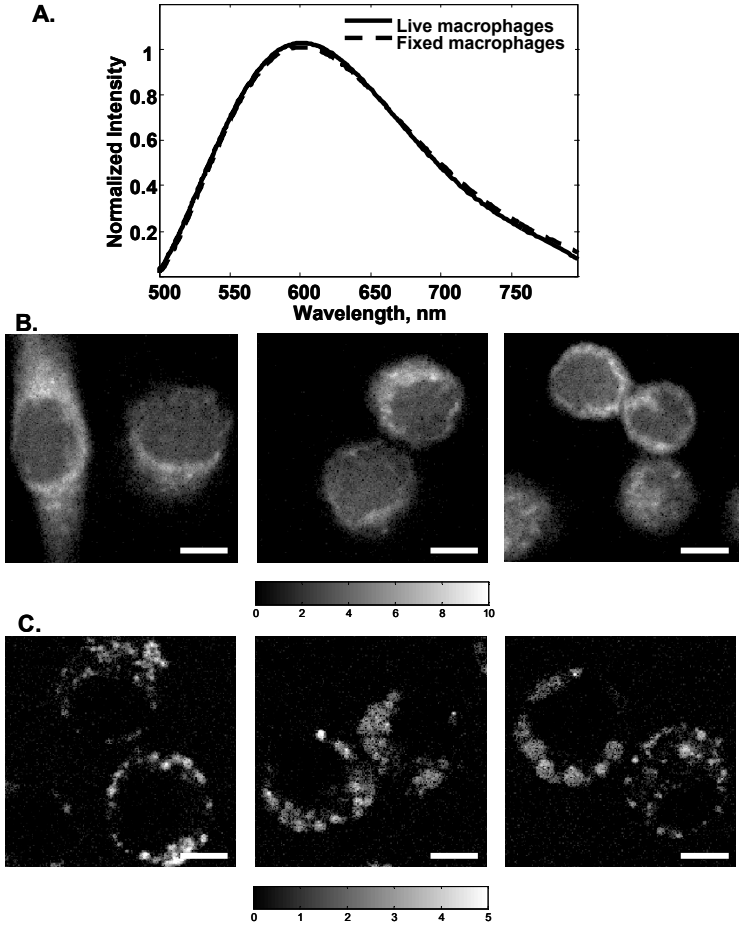

Fig. 2. Comparison of autofluorescence properties in living and fixed macrophage cells. A. Spectral signatures recovered from MCR analysis of hyperspectral imaging. B. MCR extracted concentration map of macrophage autofluorescence in fixed cells. C. MCR extracted concentration map of macrophage autofluorescence in living cells. Scale bar = 5μm.

A more comprehensive assessment of the spectral properties and emission intensity of living and fixed RAW macrophage autofluorescence is shown in Figure 3. The autofluorescence spectra identified from fixed and living RAW macrophages (Fig. 3a) were indistinguishable leading to the conclusion that the same chemical species comprise the autofluorescence in both these conditions. Though the autofluorescence may arise from the same chemical constituents, the spatial arrangement and average intensities are clearly different between fixed and living cells (Fig. 3b and 3c). Live RAW macrophages exhibit patchy areas of autofluorescence while fixed cells showed a more uniform cytoplasmic distribution and about twice the autofluorescence intensity relative to live cells as indicated in the color bars beneath the images.

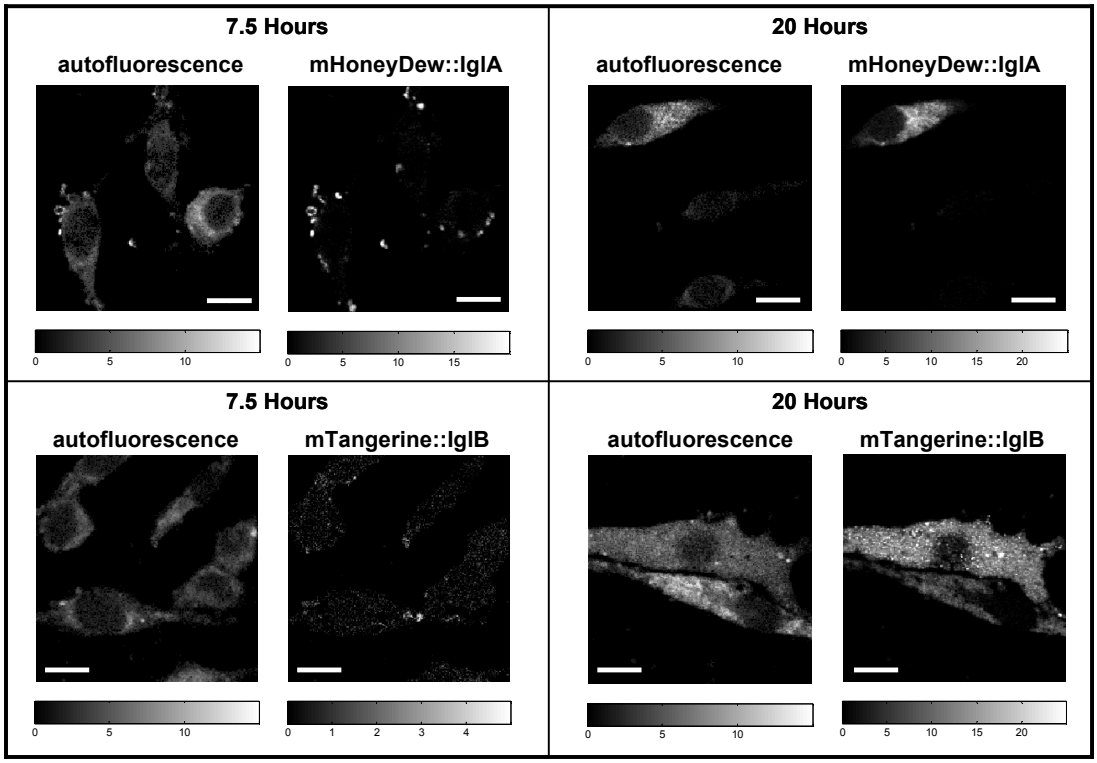

Fig. 4. Spatial distribution of mHoneydew::IglA and mTangerine::IglB expression in *F. novicida* infected macrophage cells at two different time points post-infection. Cells were fixed following infection and prior to imaging. Images shown are MCR extracted concentration maps. Scale bar = 5μm.

Figure 4 illustrates the relative intensity of macrophage autofluorescence compared to *F. novicida* protein expression at two different time points after infection. These results are part of a larger experiment designed to follow the levels of *F. novicida* protein expression in space and time. Accurate estimation of macrophage autofluorescence and subsequent removal of its contribution from the fluorescent protein images is necessary because of the low levels of protein fluorescence. For example, at the 7.5 hour time point the average intensity levels of IglA and IglB protein expression are of the same magnitude as the autofluorescence. At 20 hours post-infection, the average IglA protein expression intensity has increased to levels approximately 2-3 times that of the autofluorescence, but even at this time point IglB protein expression is on average still on the same order of magnitude as the autofluorescence (Note: The average intensity is not very different from that at t=7.5 hours) The IglB protein shows tight foci of higher concentration at the t=20 hours. Table 1 contains a summary of the image analysis statistics at these two time points. Although only one cell is shown for each of the conditions in Figure 4, the values reported in Table 1 were generated from a larger set containing separate observations of 5 cells for all timepoints and proteins except mHoneydew expression at t=20 hours which was generated

from observations of 3 cells. It should be noted that the Igl and autofluorescence areas in Table 1 are not expected to add to the cell area as these species are not mutually exclusive in their location.

Table 1. Comparison of macrophage autofluorescence and Igl protein expression intensities at two time points following *F. novicida* infection of RAW264.7 cells. Values reported are average values from five independent cell images with the exception of the mHoneydew 20 hour time point which was the average of three independent cells. To enable direct comparisons between the values, intensities were calculated from independent concentration maps previously scaled for the each spectral emission maximum =1.

	Cell Area (um^2)	AF Area (um^2)	Igl Area (um^2)	Mean AF Intensity (a.u.)	Mean Igl Intensity (a.u.)	Image Characteristics
mTangerine::IglB, 7 hrs	33.1	9.2	0.2	4.0	3.8	1-5 individual, isolated bacteria per cell
mHoneydew::IglA, 7 hrs	44.0	13.9	2.0	4.9	11.8	1-5 individual, isolated bacteria per cell
mTangerine::IglB, 20 hrs	82.0	51.4	54.3	5.9	7.8	Cells are filled with bacteria
mHoneydew::IglA, 20 hrs	54.6	28.7	29.9	9.8	16.6	Cells are filled with bacteria

4. DISCUSSION

Figure 1 and 2 illustrate the importance of spectral imaging for this fluorescent protein application. When SBT occurs a microscopist might attempt to select a different label or a different wavelength region, however visible excitation of cell and tissue autofluorescence is broad enough to interfere significantly with any of the visible fluorescent proteins. One exception is the red fluorescent proteins which are often not desirable for imaging because of their tendency to form dimers, low quantum yield, photoinstability, and maturation time.[21, 22] Spectral imaging coupled with MCR allows the unique ability to extract the spectra of the underlying fluorescent species in these spectrally overlapped images of host-pathogen interactions (without a need to know their spectral features *a priori*) and calculate independent concentration maps that locate and provide relative concentrations of each of these species. MCR has been very successful in separating signal from multiple labels and autofluorescence in tissue and microarrays[10, 23] and though not directly demonstrated by the biological experiments performed in this study, MCR is capable of resolving all four of the spectra shown in Fig.1 from the same image. The MCR algorithm assumes a linear additive relationship (Beer's Law) and the use of constraints (spectral and concentration non-negativity, etc.) ensures realistic solutions. For two components to be identified as separate species by MCR they must vary in spectral shape and/or spatial location throughout the image. Once spectra are obtained, subsequent images can be analyzed using a classical least squares algorithm. Investigation of the spectral residuals provides confidence that the spectral model is valid for new images. MCR models developed in these proceedings resulted in the autofluorescence spectra shown in Fig. 1 as well as additional spectra as appropriate to the experiment (i.e. if the unlabeled cells were imaged just the autofluorescence spectrum was used, but if cells plus bacteria were labeled with GFP were imaged then both the GFP and autofluorescence spectra were used to create the model). All models explained >99.8% of the variance in the images.

Both of the autofluorescence patterns observed in Fig. 3 are difficult at best to correct for with traditional background estimation and subtraction based on separate control samples. The live cell autofluorescence is even more problematic because it is highly variable within a cell and could not be represented accurately by any single numerical value. In addition without spectral imaging it would not be possible to determine the location of the either the mHoneydew- or mTangerine-labeled bacteria in a living cell because of this patchy, contaminating autofluorescence that is brighter than the protein expression. This would prevent imaging studies from visualizing interactions in the early stages of infection. At the much later time points, once the bacteria have replicated within the host, the expression intensity levels do increase. At these higher expression levels it is still important to accurately model the macrophage autofluorescence as

Table 1 shows. Consider the IglB expression at 20 hours post-infection. Due to their degree of spectral overlap, even then a filter-based microscope would see these two species as contributing about equally to the signal detected.

It was unexpected that the living cells and fixed cells possess the same spectral signature for autofluorescence. This indicates the same molecular moieties are contributing to the spectrum. The differences in spatial localization and intensity of macrophage autofluorescence shown in Fig. 3 are most likely due to the loss of membrane integrity in the fixation process. During fixation organelle membranes become disrupted and the autofluorescent species can leak out, filling the cytoplasm more uniformly. The results may not necessarily be the same if a different cellular system were interrogated or if a different fixation protocol were used. For example, glutaraldehyde fixation is thought to generate new fluorescent species. Spectral imaging and MCR analysis have the advantage that they can be applied to many applications to characterize the autofluorescence and prevent it from negatively affecting the results.

Although macrophage autofluorescence is often considered an inconvenience in cell based imaging applications, it does have a benefit when using a spectral imaging microscope – the autofluorescence signal can be used to generate contrast and "label" the cell, reducing the need for an additional label in an already crowded spectral space. We can easily generate color images in which we use the autofluorescence to label the cell and another color to represent the fluorescent proteins of interest (not shown).

5. CONCLUSIONS

In this work we have investigated the spectral properties of macrophage autofluorescence in living and fixed cells using a confocal spectral imaging microscope and multivariate curve resolution to perform the spectral unmixing. We have demonstrated the importance of accurate measurement of macrophage autofluorescence for our specific application following Igl protein expression during *F. novicida* infection. The relative protein expression levels are of the same magnitude of the autofluorescence at early time points (<10 hours post infection) and can even have similar spatial distribution (particularly in living cells), making it impossible to interpret images accurately without the use of spectral imaging and an unmixing analysis to separate the overlapped spectra into their underlying fluorescent species. By developing an accurate model for the autofluorescence, the images of the analytes can be effectively corrected for autofluorescence contribution. The methods developed in this work are broadly applicable to many imaging applications where spectral bleed through leads to contaminating signal.

ACKNOWLEDGMENTS

The following reagent was obtained through the NIH Biodefense and Emerging Infections Research Resources Repository, NIAID, NIH: *Francisella novicida* Type Strain, Strain Utah 112, NR-13. The authors wish to thank Roger Tsien for the fruit fluorescent proteins, Bryan Carson and Amanda Carroll-Portillo for helpful discussion about macrophage autofluorescence and cell biology, and the following people for algorithm and software development (listed alphabetically): David M. Haaland, Paul G. Kotula, Michael R. Keenan, Tony Ohlhausen, Greg Poulter, Christopher L. Stork, Mark H. Van Benthem. Sandia is a multi-program laboratory operated by Sandia Corporation, a Lockheed Martin Company, for the United States Department of Energy under Contract DE-ACO4-94AL85000.

REFERENCES

1 A. Periasamy & R. N. Day, *Molecular Imaging*, Oxford University Press, New York, 2005.

2 J. A. Timlin, M. B. Sinclair, D. M. Haaland, M. J. Martinez, M. Manginell, S. M. Brozik, J. F. Guzowski & M. Werner-Washburne, "Hyperspectral imaging of biological targets: the difference a high resolution spectral dimension and multivariate analysis can make", in *IEEE International Symposium on Biomedical Imaging*, Arlington, VA, (2004).

3 T. Zimmerman, J. Rietdorf & R. Pepperkok, "Spectral imaging and its applications in live cell microscopy", *Federation of European Biochemical Societies Letters,* **546,** 87-92, (2003).

4 X. Michalet, A. N. Kapanidis, T. Laurence, F. Pinaud, S. Doose, M. Pfughoefft & S. Weiss, "The power and prospects of fluorescence microscopies and spectroscopies", *Annual Review of Biophysics and Biomeolecular Structure,* **32,** 161-182, (2003).

5 N. Keshava & J. F. Mustard, "Spectral unmixing", *Ieee Signal Processing Magazine,* **19,** 44-57, (2002).

6 R. A. Schultz, T. Nielsen, J. R. Zavaleta, R. Ruch, R. Wyatt & H. Garner, R., "Hyperspectral imaging: A novel approach for microscopic analysis", *Cytometry,* **43,** 239-247, (2001).

[7] M. E. Dickinson, G. H. Bearman, S. Tille, R. Lansford & S. E. Fraser, "Multi-spectral imaging and linear unmixing add a whole new dimension to laser scanning fluorescence microscopy", *Biotechniques,* **31,** 1272-1278, (2001).
[8] J. R. Mansfield, K. W. Gossage, C. C. Hoyt & R. M. Levenson, "Autofluorescence removal, multiplexing, and automated analysis methods for in-vivo fluroescence imaging", *Journal of Biomedical Optics,* **10,** (2005).
[9] L. T. Nieman, M. B. Sinclair, J. A. Timlin, H. D. T. Jones & D. M. Haaland, "Hyperspectral imaging system for quantitative identification and discrimination of fluorescent labels in the presence of autofluorescence", in *2006 IEEE International Symposium on Biomedical Imaging*, Arlington, VA, (2006).
[10] J. A. Timlin, M. B. Sinclair, D. M. Haaland, A. D. Aragon, M. J. Martinez & M. Werner-Washburne, "Hyperspectral microarray scanning: Impact on the accuracy and reliability of gene expression data", *BMC Genomics,* **6,** (2005).
[11] M. J. Martinez, A. D. Aragon, A. L. Rodriguez, J. M. Weber, J. A. Timlin, M. B. Sinclair, D. M. Haaland & M. Werner-Washburne, "Identification and removal of contaminating fluorescence from commercial and in-house printed DNA microarrays", *Nucleic Acids Research,* **31,** e18, (2003).
[12] J. A. Timlin, L. T. Nieman, H. D. T. Jones, M. B. Sinclair, D. M. Haaland & J. F. Guzowski, "Imaging multiple endogenous and exogenous fluorescent species in cells and tissues", in *Imaging, Manipulation, and Analysis of Biomolecules, Cells, and Tissues IV*, San Jose, CA, USA, (2006).
[13] O. M. de Bruin, J. S. Ludu & F. E. Nano, "The Francisella pathogenicity island protein IglA localizes to the bacterial cytoplasm and is needed for intracellular growth", *BMC Microbiology,* **7,** (2007).
[14] M. B. Sinclair, D. M. Haaland, J. A. Timlin & H. D. T. Jones, "Hyperspectral confocal microscope", *Applied Optics,* **45,** 3283-3291, (2006).
[15] J. S. Ludu, E. B. Nix, B. N. Duplantis, O. M. de Bruin, L. A. Gallagher, L. M. Hawley & F. E. Nano, "Genetic elements for selection, deletion mutagenesis and complementation in *Francisella* spp." *FEMS Microbiology Letters,* epub ahead of print, (2007).
[16] P. Hing & H. W. Muller, "CCD cameras simplify biology", *Biophotonics,* 52-58, (September 2003).
[17] M. R. Keenan & P. G. Kotula, "Accounting for Poisson noise in the multivariate analysis of ToF-SIMS Spectrum Images", *Surface and Interface Analysis,* **36,** 203-212, (2004).
[18] P. G. Kotula, M. R. Keenan & J. R. Michael, "Automated analysis of SEM X-Ray spectral images: a powerful new microanalysis tool." *Microscopy & Microanalysis,* **9,** 1-17, (2003).
[19] M. H. Van Benthem & M. R. Keenan, "Fast algorithm for the solution of large scale non-negativity constrained least squares problems", *Journal of Chemometrics,* **18,** 441-450, (2004).
[20] D. M. Haaland, J. A. Timlin, M. B. Sinclair, M. H. Van Benthem, M. J. Martinez, A. D. Aragon & M. Werner-Washburne, "Multivariate curve resolution for hyperspectral image analysis:applications to microarray technology", in *Spectral Imaging: Instrumentation, Applications, and Analysis*, San Jose, CA, (2003).
[21] A. A. Heikel, S. T. Hess, G. S. Baird, R. Y. Tsien & W. W. Webb, "Molecular spectroscopy and dynamics of intrinsically fluorescent proteins: Coral red (dsRed) and yellow (Citrine)", *Proceedings of the National Academy of Sciences of the United States of America,* **97,** 11996-12001, (2001).
[22] N. C. Shaner, R. E. Campbell, P. A. Steinbach, B. N. G. Giempmans, A. E. Palmer & R. Y. Tsien, "Improved monomeric red, orange, and yellow fluorescent proteins derived from Discosoma sp. red fluorescent protein", *Nature Biotechnology,* **22,** 1567-1572, (2004).
[23] V. Sutherland, J. A. Timlin, L. T. Nieman, J. F. Guzowski, M. K. Chawla, B. Roysam, P. F. Worley, B. L. McNaughton, M. B. Sinclair & C. A. Barnes, "Advanced imaging of multiple mRNAs in brain tissue using a custom hyperspectral imager and multivariate curve resolution", *Journal of Neuroscience Methods,* **160,** 144-148, (2007).